AIAA JOURNAL
Vol. 31, No. 6, June 1993

# Aerodynamics of Maneuvering Slender Wings with Leading-Edge Separation

T. Sean Tavares*
*U.S. Air Force Wright Laboratory, Wright-Patterson Air Force Base, Ohio 45433*
and
James E. McCune†
*Massachusetts Institute of Technology, Cambridge, Massachusetts 02139*

**A nonlinear theoretical technique is presented for treating the unsteady aerodynamics of low-aspect-ratio wings with leading-edge separation in incompressible flow. Cases are treated for wings in steady flight and for those undergoing severe unsteady maneuver. The treatment extends classical slender wing theory to allow for large-scale motion along with possibly asymmetric wake development. Calculated results are presented for a variety of cases and are compared with related analyses and experiments. Examples studied include wings of delta and clipped-delta planform. Flight conditions and maneuvers treated included sideslip, sudden plunge, and rapid constant-rate roll at zero angle of attack. New results are interpreted in the light of wake history effects, a framework which provides a simplified means of interpreting the aerodynamic response in the severe maneuver case. The ability of the calculations to reproduce observed phenomena under a wide variety of conditions supports the practical usefulness of the extended slender wing treatment as a tool for gaining increased insight into the unsteady interaction between low-aspect-ratio wings and their wakes.**

## Nomenclature

$\mathcal{R}$ = aspect ratio, $B^2/S$
$B$ = net wing span
$b$ = local wing span
$\hat{b}$ = instantaneous span of wing trace projection in the crossflow plane
$C_L$ = lift coefficient
$C_l$ = roll moment coefficient
$C_N$ = normal force coefficient
$c$ = wing chord
$\dot{h}$ = plunge rate
$M$ = roll moment on wing trace
$N$ = normal force on wing trace
$p$ = pressure
$r_c$ = vortex core radius
$S$ = wing area
$t$ = time in cross plane history
$t'$ = actual time
$U_\infty$ = freestream speed
$u, v$ = velocity components in $(x, y)$ coordinate system
$\hat{u}, \hat{v}$ = velocity components in instantaneous $(\hat{x}, \hat{y})$ coordinate system
$X_0, Y_0$ = translation components of wing trace in crossflow plane
$x, y, z$ = mean or reference coordinate system
$\hat{x}, \hat{y}$ = instantaneous wing trace fixed coordinate system in crossflow plane
$Z$ = complex location in $(x, y)$ plane, $x + iy$
$\hat{Z}$ = complex location in $(\hat{x}, \hat{y})$ plane, $\hat{x} + i\hat{y}$
$Z'$ = chordwise coordinate
$\alpha$ = angle of attack
$\bar{\alpha}$ = mean or reference angle of attack
$\beta$ = sideslip angle
$\Gamma$ = circulation
$\gamma$ = vorticity on wing trace
$\kappa$ = wing trace roll angle
$\bar{\lambda}$ = emanation time of wake element
$\rho$ = fluid density
$\phi$ = velocity potential

*Subscripts and Superscripts*

0 = no-wake component
1 = wake related component
$P, S$ = pertaining to port or starboard wake
TRC = pertaining to the wing trace
$v$ = pertaining to vortex wake element
$(\dot{})$ = first derivative with respect to time, $d/dt$
$(\ddot{})$ = second derivative with respect to time, $d^2/dt^2$

Received Jan. 23, 1992; revision received Sept. 16, 1992; accepted for publication Sept. 22, 1992. Copyright © 1992 by the American Institute of Aeronautics and Astronautics, Inc. All rights reserved.

*NRC Air Force Materiel Command Research Associate, Flight Dynamics Directorate, Aeromechanics Division, Computational Fluid Dynamics Branch. Member AIAA.

†Professor, Department of Aeronautics and Astronautics. Associate Fellow AIAA.

## I. Introduction

CURRENT interest in expanding the flight envelopes of modern tactical aircraft has created an important demand for increased understanding of flows with large-scale separation and unsteadiness. Concepts such as supermaneuverability[1] call for rapid maneuver to be performed at large angles of attack and low airspeeds. A dominant class of flows pertinent to such applications are those involving powerful ordered vortical structures (wakes) shed from the leading edges of highly swept lifting surfaces. These surfaces include low-aspect-ratio wings and control surfaces, and leading-edge and forebody strakes.

This paper describes a technique which the authors have successfully applied to the study of the unsteady separated flow aerodynamics of low-aspect-ratio wings, using an approach which can best be described as "computer aided analysis." In this approach techniques of classical wing theory receive extended application with the aid of the computer. For the present problem, for example, the simple conceptual framework afforded by the Munk-Jones slender wing theory[2,3] is adopted in a form that is extended to account for the effects of large amplitude maneuver and the nonlinear, often asymmetric, development of leading-edge vortex wakes.

Although there exists a host of more exact CFD techniques, ranging in complexity from vortex-lattice[4] to Navier-Stokes[5] codes, the slender wing technique retains the appealing feature

that the instantaneous three-dimensional flow about the wing can be obtained by the superposition of two-dimensional time-dependent flows in successive crossflow planes. Using this simple framework one can gain considerable insight into the fundamentals of the unsteady interaction between low-aspect-ratio wings and their leading-edge wakes. At the same time one can, in a wide variety of cases, predict aerodynamic performance on a quantitative basis very well, obtaining results that are consistent with more elaborate computations, with flow visualization pictures, and with wind-tunnel experiments.

Maximum use is made of the analytical techniques of two-dimensional potential flow theory in setting up and solving the unsteady crossflow problem, which is the basic part of all our slender wing calculations. This feature helps to keep computer requirements modest, allowing interactive runs to be made on machines of Micro-VAX capability. As a result, we believe that the current technique can complement (and, in some cases compete with) more conventional CFD calculations. In particular, the low computational overhead may make the method attractive as a means of predicting aerodynamic loads in interdisciplinary investigations involving structural dynamics and/or flight mechanics.

The earliest extensions of slender wing theory came shortly after Jones' 1945 paper.[3] Examples of extensions which took small amplitude unsteady motion into account, albeit independently of the effects of leading-edge separation, are reported in Refs. 6–8. In the early 1950s the effects of leading- and side-edge separation were incorporated into the treatment of slender wings in steady flight. Notable examples are the calculations for rectangular wings by Cheng,[9] and for delta planforms by Brown and Michael.[10] In both of these early treatments the vortex wakes were approximated by two concentrated vortices that were connected to the wing edges by highly idealized straight line feeding sheets. Somewhat later the unsteady slender wing theory was combined with adaptations of Brown and Michael's treatment of the leading-edge wakes. These investigations are reported in Refs. 11–13.

Advances in computing capability allowed more detailed descriptions of leading-edge separation to be incorporated into the slender body treatment by using multiple discrete vortex elements to represent each vortex wake in the crossflow plane.[14,15] However, most if not all of these improved treatments of the leading-edge wakes have been applied only to the steady case, and many of these applications were limited to cases where symmetry between the two leading-edge wakes was imposed. The current technique represents a significant advance over previous slender body methods in that generalized motion of the wing is allowed along with asymmetric wake development, where appropriate.

In the following section the theoretical treatment is described. Next, a brief outline of the numerical implementation of the technique is given. The case of a simple delta in steady flight at moderate to high angle of attack is treated as an initial test case to show the effectiveness of the method. Next, a steady flight calculation for a clipped-delta planform is presented and discussed. Following that, results are presented for three severe maneuver examples; these show, respectively, the calculated responses of a delta wing to flight at high angle of attack with imposed sideslip, to rapid constant-rate roll, and to impulsively started plunging motion.

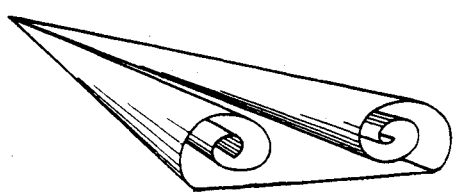

**Fig. 1 Idealized vortex wake structure above the suction surface of a slender wing.**

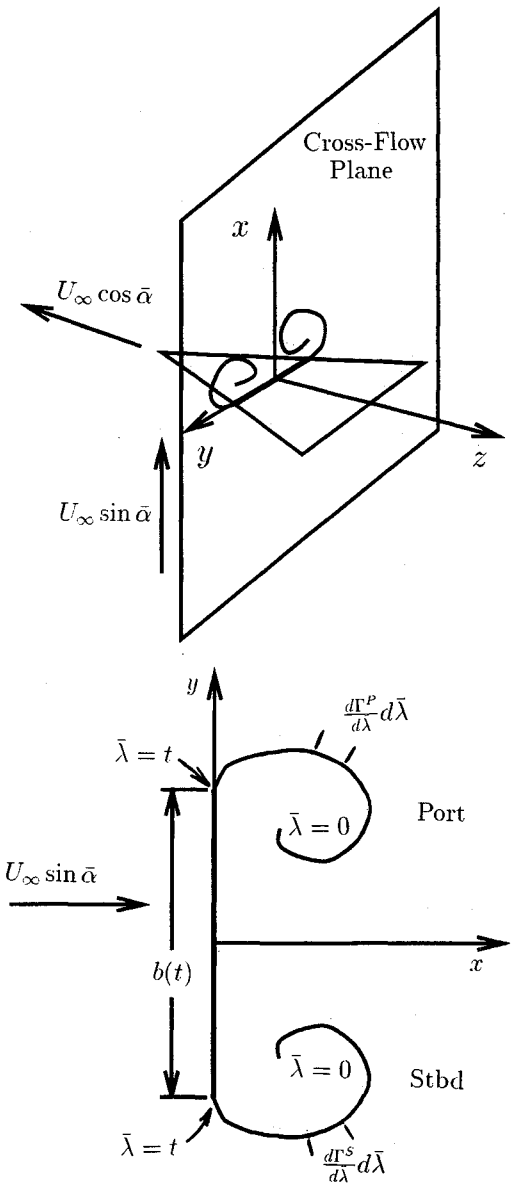


**Fig. 2 Coordinate system sketch showing time analogy frame for a slender wing in steady flight.**

## II. Theoretical Treatment

In this paper we consider infinitely thin planar wings of pointed slender planform in incompressible flow. We confine our treatment of leading-edge vortex separation to the evolution of "ideal" wakes, not addressing the formation of cores of distributed vorticity, the occurrence of secondary separation, or vortex breakdown. The wakes are modeled as thin vortex sheets emanating from sharp leading edges that are allowed to roll up subject to the condition that they remain force free. It is the general assumption that at large but finite Reynolds numbers separation occurs to maintain acceptably smooth flow at the leading edges, in a manner which, even in this context, is often called a Kutta condition (see Fig. 1).

The treatment of the problem in the slender wing limit allows an extension of the Munk-Jones "time analogy" approach to be used. This permits the three-dimensional time-dependent flow about the wing to be calculated as a superposition of two-dimensional time-dependent solutions in successive crossflow planes. We also retain trigonometric terms in angle of attack, and in roll and sideslip angles. This practice has been shown to be consistent with the concepts of slender body theory,[16] and also to give improved accuracy in cases when comparison can be made between slender body and exact three-dimensional results.[17]

Useful contact can be made with the concepts of classical unsteady airfoil theory[18,19] and its nonlinear extensions[20] in formulating and solving the resulting unsteady crossflow problem. In particular, efficient wake integral formulas for evaluating force and moment on the wing trace have been developed making use of the powerful concepts involving the Kelvin impulse of vortex systems, in a manner similar to that which was pioneered by Kármán and Sears[19] for the unsteady airfoil problem.

Figure 2 shows the coordinate system we have found effective. This is an inertial system $(x,y,z)$ through which the wing passes. The orientation of the crossflow plane is chosen such that it would lie perpendicular to the surface of a wing in steady flight at a mean or reference angle of attack, denoted $\bar{\alpha}$. We include a constant velocity crossflow in the $x$ direction of magnitude $U_\infty \sin \bar{\alpha}$, which "stops" the component of apparent plunge in the crossflow plane that would be associated with the steady flight of an uncambered wing at angle of attack $\bar{\alpha}$. This fixes the "mean" wing location in the plane $x=0$ in the reference coordinate system, while the wing advances tangent to itself in the $-z$ direction at a speed $U_\infty \cos \bar{\alpha}$. Viewed in a crossflow plane the passing of a wing in steady flight is seen as a wing trace of extent $b(t)$ that lies along the $y$ axis and that grows in time, while the intersection of the leading-edge vortex sheets and the crossflow plane form two wake traces. In this paper the symbol $t$ is used in describing events in the crossplane history, and denotes the time since the apex of the wing penetrated a particular crossflow plane. The symbol $t'$, on the other hand, denotes the "actual time" (i.e., the time coordinate used in describing the unsteady motion or response of the complete wing).

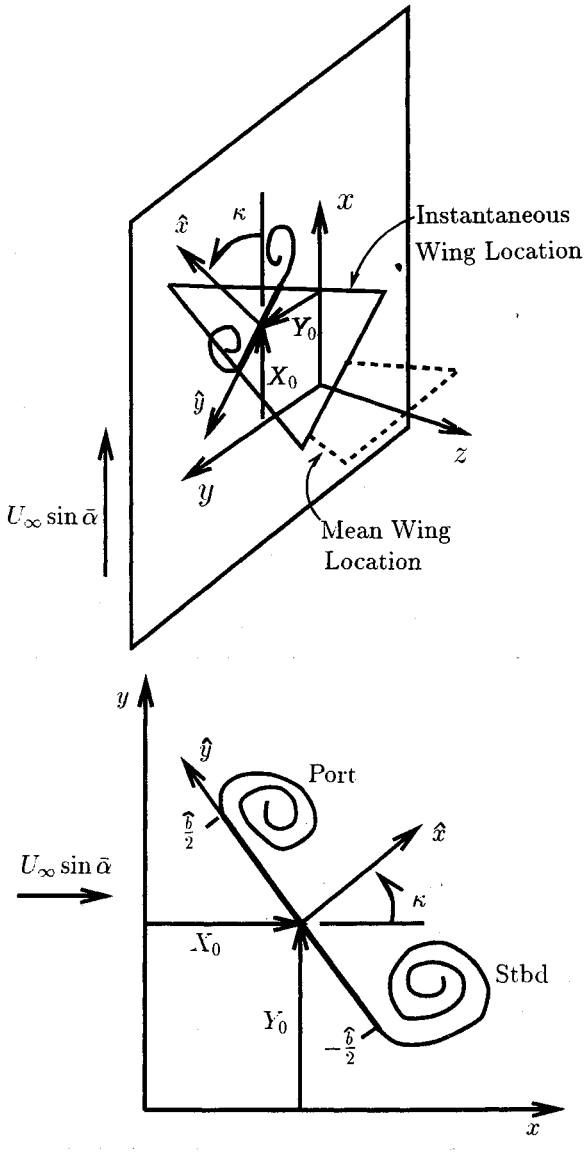


**Fig. 3 Extension to include maneuver and definition sketch for unsteady crossflow problem.**

The mathematical description of the nonlinear convection and evolution of ideal vortex wakes is contained in Refs. 20–22 and will not be repeated here. However, a synopsis of the general approach is useful. In formulating the ideal wake model the only concession to the existence of viscous-related phenomena is to enforce a Kutta condition, i.e., smooth flow, at each edge of the wing trace. Once an element of circulation has been shed, in that model, the wake is treated in the inviscid limit. Thus each increment of vorticity is convected in accordance with the inviscid Helmholtz relation.

Moreover, the ideal treatment requires that each wake trace be "force free" along its entire length. The wake vorticity then convects at the local flow velocity. In the crossflow plane this convection velocity, at any point on the wakes, is the sum of the crossflow component of the freestream, $U_\infty \sin \bar{\alpha}$, and the velocity components due to induction from the vorticity associated with the wing trace and the two wake traces.

Owing to the wake history, each element of a specified wake trace (i.e., port or starboard) can be identified according to the time it emanated from the wing edge. Denoting this time as $\bar{\lambda}$, the two wake traces at each instant $t$ in the evolution of the flow in the crossflow plane are streaklines along which $\bar{\lambda}$ varies from 0 at the far reaches of the wake traces to $t$ at the edges of the wing trace (see Fig. 2). Hence the incremental circulation associated with an element of the port or starboard wake trace, $d\Gamma^P$ and $d\Gamma^S$, respectively, can be written as $d\Gamma^P = (d\Gamma^P/d\bar{\lambda})\, d\bar{\lambda}$ and $d\Gamma^S = (d\Gamma^S/d\bar{\lambda})\, d\bar{\lambda}$. We make use of this notation in writing out the "wake history" integrals later. In Refs. 20–22 it is shown that $\bar{\lambda}$ is a "purely-convected" quantity, acting as a label for a given circulation element in the wake.

Unsteady maneuver can then be represented an an excursion about the mean wing location as sketched in Fig. 3. It is then useful to define an instantaneous $(\hat{x}, \hat{y})$ coordinate system in the crossflow plane such that the wing trace of extent $\hat{b}$ lies on the $\hat{y}$ axis, and the origin of the coordinate system coincides with the midpoint of the trace. In any cross plane the departure of the wing trace from the mean location is described by two components of translation $X_0$ and $Y_0$ and one of rotation $\kappa$. The complex locations in the two systems are related by $\hat{Z} = [Z - (X_0 + iY_0)]e^{-i\kappa}$.

### A. Determining the Vorticity on the Wing Trace

Since we are treating three-dimensional wings in the slender wing limit, the velocity and potential field in each crossflow plane is determined on a quasi-two-dimensional basis. In this limit we must calculate the two-dimensional potential solution in each crossflow plane corresponding to the vorticity concentrated on the wing trace and in the traces of the two wakes.

Transforming from the $Z$ system to the $\hat{Z}$ system, the boundary condition of no flow through the trace requires a downwash distribution along the interval $-(\hat{b}/2) \le \hat{y} \le (\hat{b}/2)$ of the $\hat{y}$ axis of strength

$$\hat{u}_{\mathrm{TRC}} = \dot{X}_0 \cos \kappa + \dot{Y}_0 \sin \kappa - \dot{\kappa}\hat{y} \tag{1}$$

In addition, Kelvin's theorem requires that the net circulation in each crossflow plane be zero. This constraint requires

$$\Gamma^P + \Gamma^S + \Gamma^{\mathrm{TRC}} = 0 \tag{2}$$

where $\Gamma^P$, $\Gamma^S$, and $\Gamma^{\mathrm{TRC}}$ denote the circulation associated with the vortex sheets representing the port and starboard wake traces and the wing trace. In the interest of distinguishing the effects of leading-edge separation, the vorticity on the wing trace is determined in two parts. The first component $\gamma_0$ is also

called the "no-wake" component, and is defined to be the noncirculatory distribution of vorticity, i.e.,

$$\int_{-\hat{b}/2}^{\hat{b}/2} \gamma_0 \, d\hat{y} = 0$$

which would satisfy boundary condition (1) in the absence of a leading-edge wake system. Using standard techniques of two-dimensional potential flow theory $\gamma_0$ is determined to be

$$\gamma_0(\hat{y}) = -2\frac{\hat{y}}{\sqrt{(\hat{b}^2/4)-\hat{y}^2}}[(U_\infty \sin\bar{\alpha} - \dot{X}_0)\cos\kappa - \dot{Y}_0 \sin\kappa] + \dot{\kappa}\left(2\sqrt{\frac{\hat{b}^2}{4}-\hat{y}^2} - \frac{\hat{b}^2/4}{\sqrt{(\hat{b}^2/4)-\hat{y}^2}}\right) \tag{3}$$

This component $\gamma_0$ would represent the complete slender wing solution for the trace vorticity if no leading-edge wakes were present.

When the leading-edge wakes are added, however, there is an additional normal component of velocity at the wing trace due to induction by the wake vortices given by

$$\hat{u}_v = -\frac{1}{2\pi}\left\{\int_0^t d\bar{\lambda}\frac{d\Gamma^P}{d\bar{\lambda}}\,\mathrm{Re}\left[\frac{i}{i\hat{y}-\hat{Z}_v^P}\right] + \int_0^t d\bar{\lambda}\frac{d\Gamma^S}{d\bar{\lambda}}\,\mathrm{Re}\left[\frac{i}{i\hat{y}-\hat{Z}_v^S}\right]\right\} \tag{4}$$

(In Eq. (4) and in subsequent equations Re[ ] denotes taking the real part of a complex quantity.) This requires an additional component of vorticity, $\gamma_1$ which produces a normal velocity distribution at the wing trace that cancels $\hat{u}_v$ exactly. The distribution of $\gamma_1$ can be gotten by standard techniques of potential flow theory using conformal mapping (i.e., by mapping the wing trace into a circle and placing image vortices to counter the downwash component associated with the wakes). For an arbitrary configuration of the wake traces and an arbitrary distribution of vorticity along them, the resulting distribution of $\gamma_1$ can be written in terms of the wake integral expression

$$\gamma_1(\hat{y}) = \frac{2}{\pi}\frac{1}{\sqrt{(\hat{b}^2/4)-\hat{y}^2}}\left\{\int_0^t d\bar{\lambda}\frac{d\Gamma^P}{d\bar{\lambda}}\,\mathrm{Re}\left[\frac{\sqrt{(\hat{Z}_v^P)^2+(\hat{b}^2/4)}}{i\hat{y}-\hat{Z}_v^P}\right] + \int_0^t d\bar{\lambda}\frac{d\Gamma^S}{d\bar{\lambda}}\,\mathrm{Re}\left[\frac{\sqrt{(\hat{Z}_v^S)^2+(\hat{b}^2/4)}}{i\hat{y}-\hat{Z}_v^S}\right]\right\} \tag{5}$$

In determining $\gamma_1$ we have enforced the constraint

$$\Gamma^{\mathrm{TRC}} = \int_{-\hat{b}/2}^{\hat{b}/2} \gamma_1 \, d\hat{y} = -(\Gamma^P + \Gamma^S)$$

so that Kelvin's theorem is satisfied.

Now, the distributions of $\gamma_0$ and $\gamma_1$, when considered separately, are both singular at the wing edges, although the assumed role of vortex separation in the first place is to cancel the leading-edge singularities that would otherwise occur.

### B. Maintaining Smooth Flow at the Wing Edges

Having determined the no-wake and wake related components of vorticity on the wing trace, and noting that the singular terms in the expressions for $\gamma_0$ and $\gamma_1$ both have $[1/\sqrt{(\hat{b}^2/4)-\hat{y}^2}]$ dependences one can ask: "What distribution of wake vorticity will exactly cancel the singularities so that $\gamma_{\mathrm{TRC}} = \gamma_0 + \gamma_1$ is finite, but not necessarily zero at each wing edge?" The answer is determined by requiring

$$\lim_{\hat{y}\to\pm\hat{b}/2}[\sqrt{(\hat{b}^2/4)-\hat{y}^2}]\,\gamma_{\mathrm{TRC}} = 0 \tag{6}$$

Expressing $\gamma_1$ in terms of its wake integral expression and applying Eq. (6) at the two wing edges then yields a pair of integral constraint equations

$$-2[(U_\infty \sin\bar{\alpha} - \dot{X}_0)\cos\kappa - \dot{Y}_0\sin\kappa] = \frac{1}{\pi}\int_0^t d\bar{\lambda}\frac{d\Gamma^P}{d\bar{\lambda}}\,\mathrm{Re}\left[\frac{i}{\sqrt{(\hat{Z}_v^P)^2+(\hat{b}^2/4)}}\right] + \frac{1}{\pi}\int_0^t d\bar{\lambda}\frac{d\Gamma^S}{d\bar{\lambda}}\,\mathrm{Re}\left[\frac{i}{\sqrt{(\hat{Z}_v^S)^2+(\hat{b}^2/4)}}\right] \tag{7}$$

and

$$-\dot{\kappa}\frac{\hat{b}}{2} = \frac{1}{\pi}\frac{2}{\hat{b}}\int_0^t d\bar{\lambda}\frac{d\Gamma^P}{d\bar{\lambda}}\,\mathrm{Re}\left[\frac{\hat{Z}_v^P}{\sqrt{(\hat{Z}_v^P)^2+(\hat{b}^2/4)}}\right] + \frac{1}{\pi}\frac{2}{\hat{b}}\int_0^t d\bar{\lambda}\frac{d\Gamma^S}{d\bar{\lambda}}\,\mathrm{Re}\left[\frac{\hat{Z}_v^S}{\sqrt{(\hat{Z}_v^S)^2+(\hat{b}^2/4)}}\right] \tag{8}$$

which must be satisfied at all times in the evolution of the wake traces to maintain smooth edge flow.

Given the geometry and motion of the wing trace, the left-hand sides of Eqs. (7) and (8) are known. The strengths of the wakes can then be determined by simultaneously solving the two equations. In fact, we note that for the unsteady crossflow problem this pair of "smooth flow constraint equations" plays a role equivalent to that played by Wagner's integral equation in unsteady airfoil theory in both its classical[18,19] and nonlinear[20] forms. Of course, a key element in calculating the kernels of the wake integrals is a knowledge of the instantaneous locations of each wake element in the port and starboard wake traces, $\hat{Z}_v^P$ and $\hat{Z}_v^S$. Our procedure for tracking the evolution of the wake traces on the computer is discussed in Sec. III.

In cases where no roll or sideslip is present, and the wakes are taken to be symmetric about the $\hat{x}$ axis, the assumed symmetry satisfies Eq. (8) exactly, and only Eq. (7) remains to be solved. This symmetric case was treated in Ref. 23. [Indeed, at the time that paper was written the analogy with Wagner's integral equation was so compelling that the symmetric form of constraint (7) was dubbed "The Cross-Flow Wagner Integral Equation."]

### C. Forces and Moments

The loading $\Delta p$ at any point on the wing trace can be calculated by straightforward application of the unsteady Bernoulli equation in the crossflow plane

$$\frac{\Delta p}{\rho} = \langle\hat{v}\rangle_{\mathrm{TRC}}(\gamma_0+\gamma_1) - \Delta\frac{\partial\phi}{\partial t} \tag{9}$$

Here $\langle\hat{v}\rangle_{\mathrm{TRC}}$ denotes the mean value of the tangential velocity evaluated at the wing trace, and $\Delta(\partial\phi/\partial t)$ denotes the difference between the rates of change of velocity potential evaluated on the bottom and top sides at any spanwise location $\hat{y}$.

However, if one is concerned primarily in making calculations of aerodynamic performance, it is useful to in effect integrate the loading beforehand by starting with the concepts of the Kelvin impulse of paired vortex systems. This step allows one to bypass the calculation of the loading at several points on the trace which would then necessitate subsequent integrations to obtain net forces and moments. The result is a substantial savings in numerical effort. For the no-wake components of force and moment, that is, those which would occur in the absence of a leading-edge wake system, this step amounts to calculating the apparent mass of the wing trace in the spirit of Refs. 3 and 8, and can be written down exactly in terms of the rate of growth of the span of the wing trace in the crossflow plane and its instantaneous motion. The no-wake component of normal force is given by

$$N_0(t) = \rho\pi\frac{d}{dt}\left\{\left(\frac{\hat{b}}{2}\right)^2[(U_\infty\sin\bar{\alpha}-\dot{X}_0)\cos\kappa - \dot{Y}_0\sin\kappa]\right\} \tag{10}$$

whereas the no-wake component of the moment taken about the center of the trace (counterclockwise positive) is given by

$$M_0(t) = -\rho\frac{\pi}{2}\left(\frac{\hat{b}}{2}\right)^2\{[(U_\infty \sin\bar{\alpha} - \dot{X}_0)^2 - \dot{Y}_0^2]\sin 2\kappa + (U_\infty \sin\bar{\alpha} - \dot{X}_0)\dot{Y}_0 \cos 2\kappa\} - \rho\dot{\kappa}\frac{\pi}{4}\left(\frac{\hat{b}}{2}\right)^3\frac{d\hat{b}}{dt} - \rho\ddot{\kappa}\frac{\pi}{8}\left(\frac{\hat{b}}{2}\right)^4 \quad (11)$$

The wake-related components of force and moment are expressible in terms of wake integrals and are given by

$$N_1(t) = -\frac{d}{dt}I_{\hat{x}1} + \dot{\kappa}I_{\hat{y}1} \quad (12)$$

and

$$M_1(t) = -\frac{d}{dt}I_{\hat{m}1} + [(U_\infty \sin\bar{\alpha} - \dot{X}_0)\sin\kappa + \dot{Y}_0\cos\kappa]I_{\hat{x}1} + [(U_\infty \sin\bar{\alpha} - \dot{X}_0)\cos\kappa - \dot{Y}_0\sin\kappa]I_{\hat{y}1} \quad (13)$$

respectively. The quantities $I_{\hat{x}1}$, $I_{\hat{y}1}$, and $I_{\hat{m}1}$ are, in effect, "moments of vorticity" calculated in the $(\hat{x}, \hat{y})$ coordinate system and are given by

$$I_{\hat{x}1}(t) = \rho\int_0^t d\bar{\lambda}\frac{d\Gamma^P}{d\bar{\lambda}}\hat{y}_v^P + \rho\int_0^t d\bar{\lambda}\frac{d\Gamma^S}{d\bar{\lambda}}\hat{y}_v^S + \rho\int_{-\hat{b}/2}^{+\hat{b}/2} d\hat{y}\hat{y}\gamma_1 \quad (14)$$

$$I_{\hat{y}1}(t) = -\rho\int_0^t d\bar{\lambda}\frac{d\Gamma^P}{d\bar{\lambda}}\hat{x}_v^P - \rho\int_0^t d\bar{\lambda}\frac{d\Gamma^S}{d\bar{\lambda}}\hat{x}_v^S \quad (15)$$

and

$$I_{\hat{m}1}(t) = -\frac{\rho}{2}\int_0^t d\bar{\lambda}\frac{d\Gamma^P}{d\bar{\lambda}}[(\hat{x}_v^P)^2 + (\hat{y}_v^P)^2] - \frac{\rho}{2}\int_0^t d\bar{\lambda}\frac{d\Gamma^S}{d\bar{\lambda}}[(\hat{x}_v^S)^2 + (\hat{y}_v^S)^2] - \frac{\rho}{2}\int_{-b/2}^{+\hat{b}/2} d\hat{y}(\hat{y})^2\gamma_1 \quad (16)$$

Making use of the wake integral expression (5) for $\gamma_1$, the quantities $I_{\hat{x}1}$ and $I_{\hat{m}1}$ can be re-expressed as

$$I_{\hat{x}1}(t) = -\rho\int_0^t d\bar{\lambda}\frac{d\Gamma^P}{d\bar{\lambda}}\mathrm{Re}\left[i\sqrt{(\hat{Z}_v^P)^2 + \frac{\hat{b}^2}{4}}\right] - \rho\int_0^t d\bar{\lambda}\frac{d\Gamma^S}{d\bar{\lambda}}\mathrm{Re}\left[i\sqrt{(\hat{Z}_v^S)^2 + \frac{\hat{b}^2}{4}}\right] \quad (17)$$

and

$$I_{\hat{m}1}(t) = -\rho\int_0^t d\bar{\lambda}\frac{d\Gamma^P}{d\bar{\lambda}}\left\{(\hat{x}_v^P)^2 - \frac{1}{2}\mathrm{Re}\left[\hat{Z}_v^P\sqrt{(\hat{Z}_v^P)^2 + \frac{\hat{b}^2}{4}}\right]\right\} - \rho\int_0^t d\bar{\lambda}\frac{d\Gamma^S}{d\bar{\lambda}}\left\{(\hat{x}_v^S)^2 - \frac{1}{2}\mathrm{Re}\left[\hat{Z}_v^S\sqrt{(\hat{Z}_v^S)^2 + \frac{\hat{b}^2}{4}}\right]\right\} \quad (18)$$

It should be emphasized that derivatives of $I_{\hat{x}1}$, $I_{\hat{y}1}$, and $I_{\hat{m}1}$ with respect to time in Eqs. (12) and (13) are taken in a coordinate system *moving with* the wing trace. Proper account has been taken in their derivation of the noninertial effects due to the motion of the wing trace relative to the inertial frame. The necessary steps are given in more detail in Ref. 21. These expressions, so treated, provide the net wing force and moment in each cross plane including the effects of the wakes.

The integrated three-dimensional, full-wing force and moments acting on the wing are then obtained by chordwise integrations involving the appropriate instantaneous forces and moments from the crossflow calculations. For example, for a wing in steady flight at angle of attack $\alpha$ and at zero sideslip one obtains, as expected, the expression for the no-wake component of the normal force, viz., $C_{N0} = \pi\mathcal{A}/2 \sin\alpha\cos\alpha$, which, for small angle of attack, reduces to the classical slender wing result.[3] Likewise, in the case of small amplitude unsteady motion of a slender delta, calculation of the no-wake contributions to the stability derivatives reproduces the well-known results of Ref. 8. The dramatic effects of the wakes, both for the steady large $\alpha$ case and for the maneuver examples, are discussed subsequently in connection with the new results reported.

### D. Initial Response to Impulsive Motion

The prediction for the force exerted on a wing in the instant just following the commencement of impulsively started motion can be difficult to calculate numerically owing to its initially singular nature. Fortunately, such singular situations often lend themselves to exploration by other means of analysis. This situation provides a case in point, and in this section a means of predicting the force on a wing in the instant just following the start of impulsive plunge is developed. It is assumed that at time $t' = 0$ the wing begins plunge normal to the $x = 0$ plane at a constant rate $\dot{h}$ ($\dot{h}$ is taken positive in the direction of the $x$ axis). The initial flight condition in this case is steady flight at constant angle of attack and zero sideslip, which means that there is a fully-developed leading-edge wake system already in existence above the wing when the plunging motion begins.

At the start of the motion, the boundary condition that no flow pass through the wing trace requires an instantaneous adjustment of the vortex system representing the wing trace and wakes such that an additional uniform downwash component of magnitude $\dot{h}$ be produced. It is reasoned, in addition, owing to the requirement for smooth flow at the wing edges, and also because the wake elements immediately adjacent to the wing edges lie nearly in the plane of the wing trace, that the additional component of downwash must be continuous at the wing edges, and extend to the first elements of the wake.

It follows that the additional vorticity distribution, associated with the wing trace and these first wake vortex elements, is equivalent to that associated with a flat plate plunging at a rate $\dot{h}$ whose semispan is expanding; not at the rate at which the actual wing trace is expanding in the crossflow plane but, rather, at the rate at which newly shed vortex elements are convected spanwise. Let us call this rate $\langle v\rangle_T$. Now if the plunge rate is sufficiently small, i.e., if $|(\dot{h}/U_\infty \sin\bar{\alpha})| \ll 1$, the quantity $\langle v\rangle_T$ can be taken to be that which would occur in the absence of plunge. This, of course, is just the component of velocity tangent to the wing trace due to induction from the wake traces present when the plunging motion begins.

The reasoning used in this argument is analagous to that used in Refs. 24 and 25 to predict the initial response to an impulsive start in linearized wing theory, in the case when no leading-edge separation is present. The jump in normal force on the wing trace $\Delta N$ is proportional to the rate of change of apparent mass of this "equivalent plate" and is proportional to the rate at which it grows, i.e., to the speed at which wake elements move tangentially, $\langle v\rangle_T$. The expression for $\Delta N$ so developed includes contributions of both the no-wake component and the wake-related component, and is given in the limit by

$$\Delta N = -\rho\pi\dot{h}b\langle v\rangle_T \quad (19)$$

in each crossflow plane, at the appropriate instant of the cross plane history corresponding to the time $t' = 0^+$. This result has been verified by the more formal application of our present theory to the impulsive plunge case and is discussed in this context in Ref. 21. The net increment of normal force exerted on the complete wing can then be obtained by integrating the individual contributions from each crossflow plane along the chord of the planform. The change in normal force coefficient at $t' = 0^+$, $\Delta C_N(0^+)$ is given by

$$\Delta C_N(0^+) = -2\pi\left[\frac{\dot{h}}{U_\infty}\right]\frac{1}{S}\int_0^c\left(\frac{\langle v\rangle_T}{U_\infty}\right)b\,dz' \quad (20)$$

In this limiting case this relationship shows how strongly the magnitude of $\Delta C_N$ depends upon conditions determined by the vortex system that exists beforehand. In addition, the result suggests that it might be useful to explore ways of controlling $\langle v \rangle_T$ in the interest of tailoring the aerodynamic response to rapid maneuver.

## III. Implementation

The foregoing treatment of the unsteady crossflow problem has been incorporated into an efficient computer routine. This routine is the basis of all our slender wing calculations and is called by a variety of interactive host programs. Using these host programs, a user is able to "fly" a wing of chosen planform in a variety of steady flight conditions and through maneuvers. These codes orchestrate the input motions for each of the crossflow plane calculations and carry out the necessary postprocessing and plotting of results, and animation of wakes.

The numerical calculation in each crossflow plane commences at the instant the apex of the wing penetrates the plane and proceeds in small time steps until the trailing edge passes through. During the calculation the evolution of each wake trace is followed, and the calculations necessary for obtaining the force and moment on the wing trace are carried out.

At each time step, a new vortex element is introduced into each wake trace to continue to maintain smooth flow at each edge. The location of these elements is determined by interpolating the shape of the wake streakline for the interval between the wing edge and the present location of the vortex element shed in the previous time step. This procedure amounts to constructing the wake's "drift time field"[20,22,26] in this interval. Details of this procedure are given in Ref. 21. Then the strengths of each of the two new wake elements are determined by simultaneously solving the two smooth flow constraint Eqs. (7) and (8). Once the strengths of these elements have been obtained, the wake integrals used to determine the instantaneous values of the linear and angular impulse can be calculated.

Next, the wakes are allowed to deform subject to the condition that each wake element be force free. Convection of the wake elements is carried out in a series of small time substeps which are nested within the main time step in which the vortex elements are shed. At each substep the velocity of each vortex element is determined as the sum of the mean crossflow velocity and the velocity components due to induction from the vorticity distributions representing the wing trace and the wake traces, as given by the Biot-Savart law. The elements are then stepped to new locations using a forward Euler scheme. The procedure of subdividing time steps is based on the idea that the temporal resolution needed to adequately capture vortex sheet rollup may be somewhat finer, for numerical purposes, than the assumed interval at which vortex elements are shed. In addition to allowing better resolution of rollup, this technique helps to prevent vortex elements being spuriously convected through the wing trace. A similar procedure was employed in the slender wing calculations reported in Ref. 16. The number of substeps per vortex shedding time step is a user-chosen parameter.

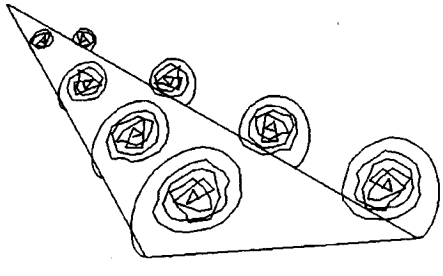

**Fig. 4 Calculated wake traces at four equally-spaced chordwise locations above an $\mathcal{R} = 0.7$ delta wing at $\alpha = 20$ deg.**

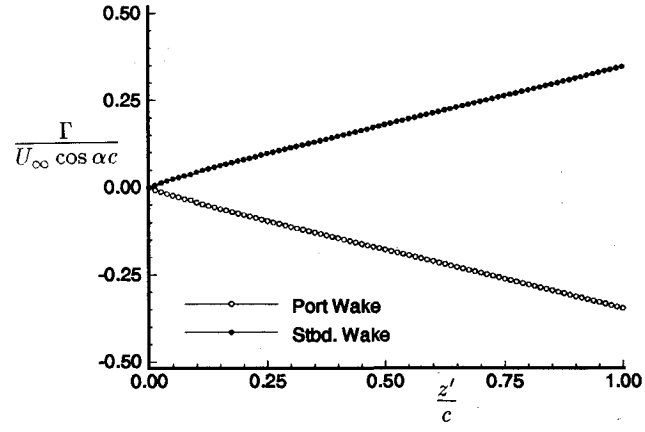


**Fig. 5 Chordwise growth of wake strengths above an $\mathcal{R} = 0.7$ delta wing at $\alpha = 20$ deg.**

In the present codes the wake traces are represented by a series of discrete vortices, each having a finite, but small axisymmetric constant vorticity (i.e., Rankine) core. The role of the cores is to prevent unrealistically large "induced" velocity components from occurring near a vortex element. Although most of the various computational methods which are available for representing vortex sheets embedded in potential flow[27] are compatible with the present analysis, the discrete vortex method has a long history, and was chosen for its simplicity and flexibility. The core radius is a user-specified parameter, which is the same for all vortex elements, and which remains constant throughout the calculation.

As is the case for most numerical methods with vortices, for any given problem the "best" values of the aforementioned user-specified parameters are determined by experience. However, the choice of a reasonable range of vortex core radii can be guided by dimensional arguments. For example, for the crossflow problem corresponding to the case of a delta wing in steady flight at zero sideslip, the vortex strength of one of the wake traces at an instant $t$ is of the order of the product of the mean crossflow velocity and the instantaneous span of the wing trace. This scaling can be verified by the calculations of Ref. 10, for example. The incremental circulation associated with a typical vortex element $\Delta\Gamma$ is then characterized by the wake trace circulation divided by the population of vortices present. For an isolated Rankine vortex, the maximum tangential speed occurs at the edge of the vortex core and is given by $V_{\max} = (\Delta\Gamma/2\pi r_c)$ where $r_c$ is the radius of the core. If one then chooses an upper limit of $V_{\max}$, a "reasonable" value being on the order of the mean crossflow velocity, one can use the given relationship to choose $r_c$.

For typical calculations, in which 60–100 vortices are introduced per cross plane, the ratio of core radius to maximum wing trace span ranges from 0.001 to 0.005, and 5–10 substeps per vortex shedding time step are used. A parametric study performed in Ref. 21 showed such key quantities as wake centroid location, wake strength (circulation), and normal force to be virtually independent of the actual value of the core radius when such small cores were used. These quantities were also insensitive to the number of substeps used in the time-stepping scheme, for a range of 5–20 substeps per vortex shedding time step.

Calculation of the evolution of vortex wakes above a simple delta in steady flight at constant angle of attack is a particularly useful test case for checking the effectiveness of the numerical technique. Figure 4 illustrates calculated "streaklines" at four chordwise intervals for a delta wing with 80-deg leading-edge sweep ($\mathcal{R} = 0.7$) at 20-deg angle of attack and zero sideslip. In this example 80 vortices were introduced to represent each wake by the time the final step in the calculation was completed. In our studies symmetry of the wake structure about the wing centerline was not imposed but emerged as a result of the calculation. Evident in the examples

shown is the occurrence of jagged vortex patterns as one moves more and more toward the inner portion of the rolled up wake. This tendency toward disorder is a well-known problem with the discrete vortex representation.[27] It results in part because of too few vortices being used, and/or too coarse a time step to resolve the rapid and highly curved vortex element trajectories in the inner wake region. Additionally, these inner elements, since they have been adrift the longest, suffer the largest cumulative effects of numerical instabilities and truncation errors in the integration scheme. Despite its jaggedness, however, this wake representation, as we verify in the results to follow, has proven to be entirely adequate for purposes of making aerodynamic performance calculations of the kind being reported here.

Within the strictly slender limit an essential feature of the flow about a simple delta is conical self similarity. This implies that the circulation associated with each wake grows linearly with chordwise distance from the apex. As seen in Fig. 5 this feature of conical flow is well represented by the corresponding calculation.

The use of an array of discrete vortices to describe a continuous vortex sheet is well recognized to be a far from perfect representation. It may therefore be necessary and/or desirable for a wider range of applications to implement a more sophisticated wake model. There are many available "fixes" for the discrete vortex model which could be explored,[27] although the

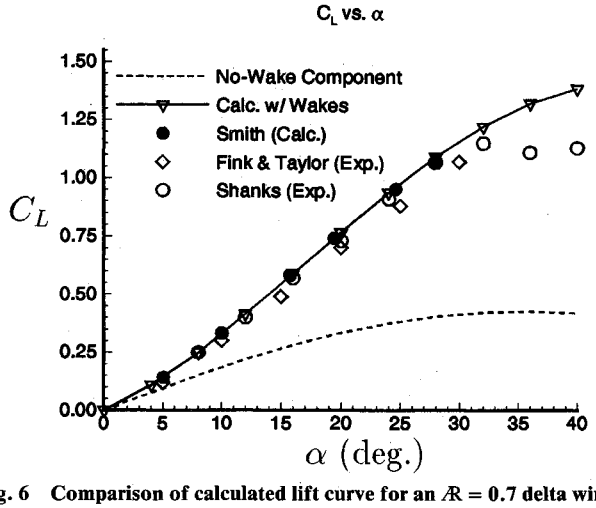


**Fig. 6 Comparison of calculated lift curve for an $\mathcal{R} = 0.7$ delta wing with Smith's calculations and wind-tunnel experiments.**

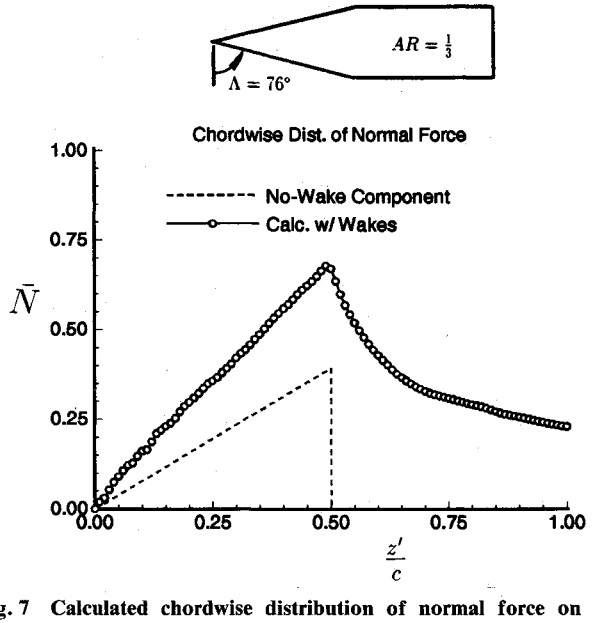


**Fig. 7 Calculated chordwise distribution of normal force on an $\mathcal{R} = \frac{1}{3}$ clipped delta at $\alpha = 15$ deg.**

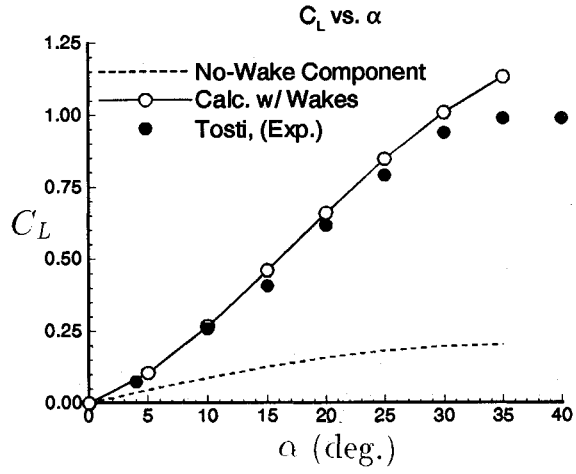


**Fig. 8 Comparison of calculated and measured lift curves for an $\mathcal{R} = \frac{1}{3}$ clipped delta wing.**

root of many of the problems with this method seems to lie in its nonconvergent representation of the near-field velocity. Probably the most dramatic possibility for improvement in resolution of wake rollup is offered by a vortex panel method such as that developed by Hoeijmakers.[28] However, in adopting any of the more sophisticated schemes one should address the effect of any procedure that redistributes wake vorticity, for example, amalgamating vortex elements into a core in tightly rolled up regions, on the dynamics of the system. In particular, one would want to ensure that any redistribution does not introduce unacceptable jumps in the calculation of the growth of wake strength, or of those components of force and moment that depend on the differentiation of wake integrals.

## IV. Results

As a first example of a calculation of the aerodynamic performance of a slender wing, a comparison of calculated vs measured[29,30] lift curves for a delta with 80-deg leading-edge sweep is shown in Fig. 6. The portion of lift that would occur in the absence of leading-edge vortices is also shown to emphasize the large component of vortex lift augmentation that actually occurs even at moderate angles of attack. As seen in the figure, the results of the present calculation are practically indistinguishable from the well-known slender wing conical flow calculations by Smith.[15]

The comparison with experiment shows excellent correspondence between our calculations and measurements, for angles of attack up to about 30 deg. Beyond that, the onset of stalling is seen, a phenomenon which, of course, is not included in the present model. This level of agreement indicates that the present model contains an adequate and useful representation of the physics needed to predict aerodynamic performance accurately under a wide variety of conditions.

The treatment is equally applicable to other pointed, slender planforms. Figure 7 shows the chordwise distribution of normal force on a clipped delta planform of aspect ratio 1/3 at 15-deg angle of attack. The force is plotted in nondimensional form, with $\bar{N} \equiv (N/\frac{1}{2}\rho U_\infty^2 B)$. This planform consists of a delta of 76-deg leading-edge sweep which has been clipped to a planform having constant span aft of the 50% root chord location. As illustrated the no wake contribution to the lift drops to zero aft of the kink, consistent with Jones' slender wing theory. On the other hand, the net lift per unit chord grows linearly on the forward portion of the wing, and trails off aft of the 50% point. The shape of the force distribution aft of the kink is somewhat reminiscent of Cheng's[9] result for the low-aspect-ratio rectangular wing.

In Fig. 8 comparison is made with a wind-tunnel measurement on a wing of this planform from Ref. 31. Again, the

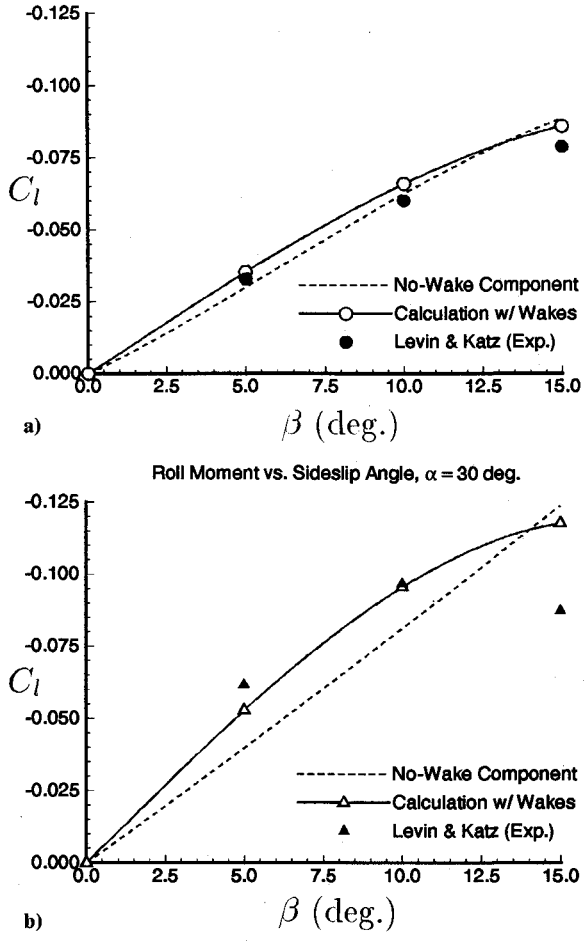


**Fig. 9 Comparison of predicted and measured roll moments on an $\mathcal{R} = 0.7$ delta wing in large amplitude sideslip: a) $\alpha = 20$-deg case and b) $\alpha = 30$-deg case.**

comparison between our calculations and experiment is excellent for angles of attack up to about 30 deg. Such agreement is particularly encouraging since the presence of leading-edge separation accounts for virtually all of the lift at higher angles of attack.

Figure 9 shows a comparison of calculated and measured roll moments for a delta with 80-deg leading-edge sweep undergoing sideslip.[32] Again, the calculated no-wake component of the roll moment is plotted for comparison, and it is rather remarkable that even though the leading-edge wakes contribute a large fraction to the lift at the angles of attack shown, the wake vortices turn out to contribute a rather small fraction of the overall rolling moment. At $\alpha = 20$ deg, the comparison with experiment is excellent for the entire range of sideslip angles explored. It is also good for angles of sideslip up to 10 deg when $\alpha = 30$ deg. (Note that for this planform at 10 deg sideslip the port wing edge is parallel to the incoming flow.) For sideslip greater than 10 deg the agreement is not good. A likely reason for this discrepancy between calculated and measured roll moments at the larger angles of sideslip and higher angles of attack is the occurrence of vortex bursting on the windward wing edge.

Figure 10 shows the chordwise development of wakes shed from the edges of an $\mathcal{R} = 0.7$ delta undergoing rapid constant rate roll at zero angle of attack. The roll rate is such that the wing completes one 360 deg roll in the time it takes to travel 1.1 chord lengths. Not surprisingly, as seen in the cross section of the wake plotted in the lower half of the figure, the wake patterns show what might be called perfect antisymmetry. Again, this wake configuration is not imposed but is allowed to emerge as a result of the calculation. Moreover, the wakes are markedly nonconical. At the more forward chordwise stations, the wakes are confined to the region close to the wing edges. As one moves back from the apex, however, the tangential speed of the tips increases due to the increasing local span and the wake becomes fuller, and the rolled up "core" moves inward toward the wing centerline.

Figure 11 is a comparison of calculated and measured[33] chordwise distribution of rolling moment for the same wing rolling at a nondimensional roll rate of $(\kappa B/2U_\infty) = 0.3$. The roll moment distribution is plotted in nondimensional form, with $\bar{M} \equiv (M/\frac{1}{2}\rho U_\infty^2 B^2)$. Also plotted is the no-wake component of the roll moment. As seen in the figure, the correspondence between the calculated roll moment and the available data for this case is good, back to the ¾ root chord location. Aft of this point the local failure of the slender wing approximation (due to its inability to account for a trailing-edge Kutta condition) gives rise to an increasing discrepancy between the calculation and experiment.

The response of an $\mathcal{R} = 0.7$ delta wing to a sudden change in its angle of attack from 20 to 25 deg, as brought about by impulsively started constant rate plunge is shown in Figs. 12 and 13. Figure 12 illustrates the response of the wakes at the

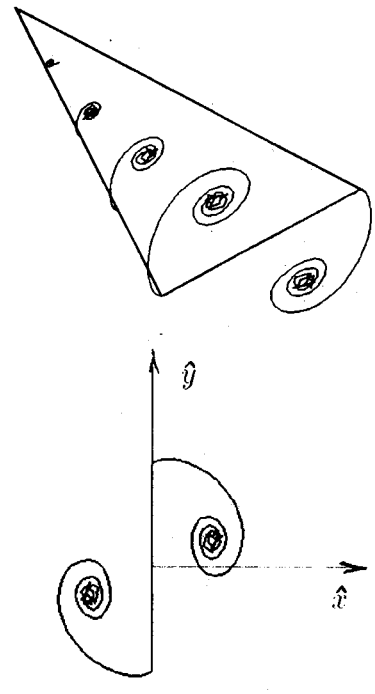


**Fig. 10 Chordwise development of wakes about an $\mathcal{R} = 0.7$ delta wing in rapid constant rate roll, and view of wake traces at trailing-edge location in the crossflow plane.**

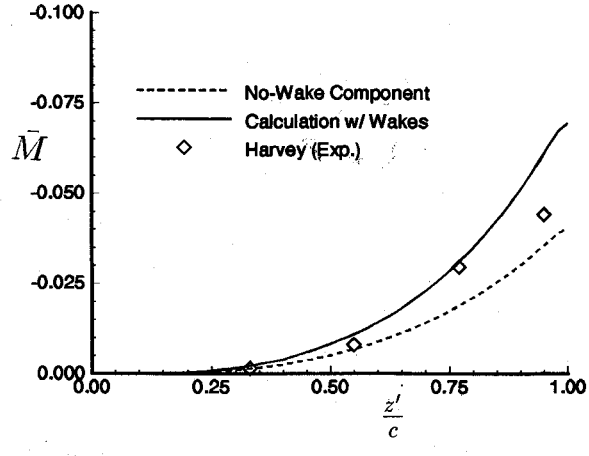


**Fig. 11 Chordwise distribution of roll moment on a rapidly rolling $\mathcal{R} = 0.7$ delta wing.**

wing trailing edge and the growth in wake strength over the time that it takes for the wing to advance one chord length. In the figures $\bar{t}'$ denotes the nondimensional time ($t' U_\infty \cos \bar{\alpha}/c$). The intensification of the two wakes (i.e., the increase in their circulation) at a fixed chordwise station is reflected dramatically in the pinching of the feeding sheet to the extent that a distinct "second vortex" is formed which migrates up the feeding sheet and is eventually swallowed by the main vortex core. This second vortex signature was observed by Lambourne et al. as reported in Ref. 34.

Figure 13 shows the corresponding transient in the normal force exerted on the wing. The complete response with the effects of wakes included contrasts sharply with the form of the no-wake component which jumps instantaneously to the steady-state value at the new effective angle of attack. In contrast, when the effects of wakes are included, the response is characterized by an initial overshoot beyond the eventual steady-state lift followed by a gradual relaxation. The symbol labeled Prediction for $t' = 0^+$ indicates the calculation given in Eq. (20) that matches the magnitude of the change in normal force quite well.

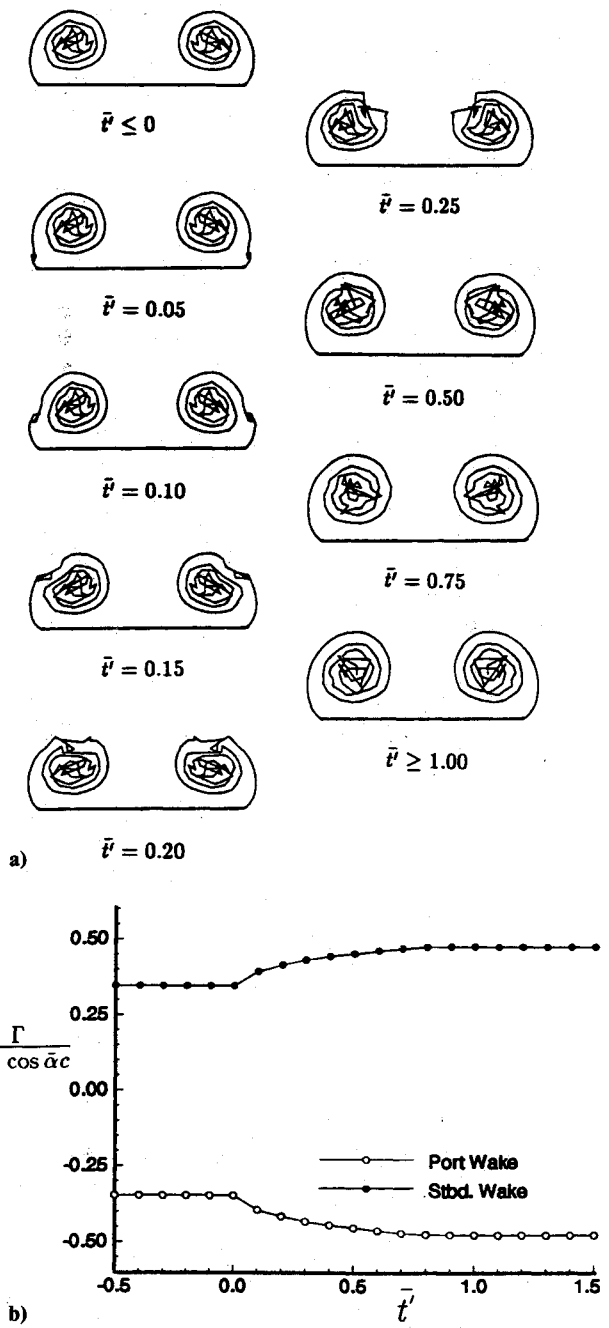


**Fig. 12 Response of wakes above an $\mathcal{R} = 0.7$ delta wing to impulsively started constant rate plunge: a) time history of wakes at the trailing edge and b) time history of wake circulation at wing trailing edge.**

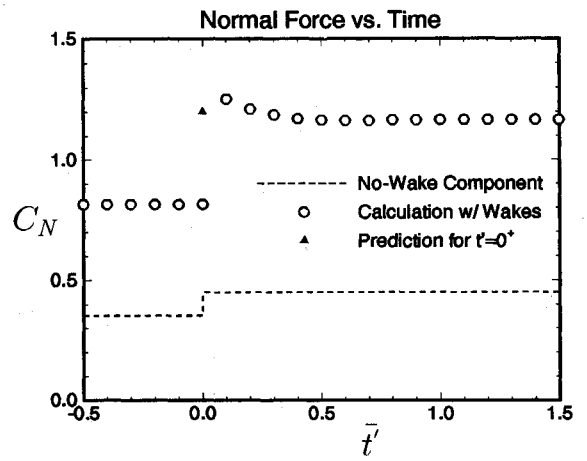


**Fig. 13 Normal force response following impulsively started plunge for an $\mathcal{R} = 0.7$ delta wing.**

## V. Conclusions

A computer-enhanced analytic technique has been developed for calculating the response of slender wings to large amplitude imposed motion, both steady and unsteady. The technique combines an extension of the concepts of slender wing theory, with techniques from two-dimensional unsteady airfoil theory for the description and treatment of the leading-edge wakes.

The current technique is intended for the study of rapid and large-scale motion of slender wings and their aerodynamic response. It has been successfully implemented for a variety of cases, and it is believed that the insights gained using this simplified treatment can complement investigations involving the use of more exact CFD methods and experiments. Furthermore, the modest computer requirements of the technique may make it attractive for use in interdisciplinary investigations combining aerodynamics, structures, and flight mechanics.

## Acknowledgments

This study was supported in part by AFOSR Grants 86-157 and 87-NA-249. William R. Sears provided us with many valuable insights and much inspiration during the course of this research. We wish to thank him for his interest in this work and are pleased to dedicate this paper to him in honor of his 80th birthday.

## References

[1]Herbst, W. B., "Future Fighter Technologies," *Journal of Aircraft,* Vol. 17, No. 8, 1980, pp. 561–565.

[2]Munk, M., "The Aerodynamic Forces on Airship Hulls," NACA Rept. 184, 1924.

[3]Jones, R. T., "Properties of Low-Aspect-Ratio Pointed Wings Below and Above the Speed of Sound," NACA Rept. 835, May 1945.

[4]Konstadinopoulos, P., Thrasher, D. F., Mook, D. T., Nayfeh, A. H., and Watson, L., "A Vortex-Lattice Method for General Unsteady Aerodynamics," *Journal of Aircraft,* Vol. 22, No. 1, 1985, pp. 43–49.

[5]Kandil, O. A., and Chuang, H. A., "Unsteady Navier-Stokes Computations Past Oscillating Delta Wings at High Incidence," AIAA 27th Aerospace Sciences Meeting, AIAA Paper 89-0081, Reno, NV, Jan. 1989.

[6]Garrick, I. E., "Some Research on High-Speed Flutter," *Proceedings of the Third Anglo-American Aeronautical Conference,* Royal Aeronautical Society, Brighton, England, UK, 1952, pp. 419–446.

[7]Miles, J. W., "Slender Body Theory for Supersonic Unsteady Flow," *Journal of the Aeronautical Sciences, Readers' Forum,* Vol. 19, No. 4, 1952, pp. 280–281.

[8]Ribner, H. S., "The Stability of Low-Aspect-Ratio Triangular Wings at Subsonic and Supersonic Speeds," NACA TN 1423, July 1947.

[9]Cheng, H. K., "Remarks on Nonlinear Lift and Vortex Separation," *Journal of the Aeronautical Sciences, Readers' Forum,* Vol. 21, No. 3, 1954, pp. 212–214.

[10]Brown, C. E., and Michael, W. H., "On Slender Delta Wings with Leading-Edge Separation," NACA TN 3430, Jan. 1955.

[11]Dore, B. D., "Non-Linear Theory for Slender Wings in Sudden Plunging Motion," *Aeronautical Quarterly,* Vol. XVII, May 1966, pp. 187–200.

[12]Lowson, M. V., "The Separated Flow on Slender Wings in Unsteady Motion," British Aeronautical Research Council, ARCR&M, No. 3448, London, Sept. 1963.

[13]Randall, D. G., "Oscillating Slender Wings with Leading-Edge Separation," *Aeronautical Quarterly,* Vol. XVII, Nov. 1966, pp. 311–331.

[14]Sacks, A. H., Lundberg, R. E., and Hanson, C. W., "A Theoretical Investigation of the Aerodynamics of Slender Wing-Body Combinations Exhibiting leading-Edge Separation," NASA CR-719, March 1967.

[15]Smith, J. H. B., "Improved Calculations of Leading-Edge Separation from Slender Thin Delta Wings," *Proceedings of the Royal Society of London,* Ser. A, Vol. 306, The Royal Society, London, 1968, pp. 67–90.

[16]Cheng, H. K., Edwards, R. H., Jia, Z. X., and Lee, C. J., "Vortex Dominated Slender-Wing Problems: Studies by a Point Vortex Method," AIAA Paper 88-3744, July 1988; also *Proceedings of the 1st National Fluid Dynamics Congress,* AIAA, Washington, DC, 1988, pp. 512–522.

[17]Hemsch, M. J., "Comparison of High-Angle-of-Attack Slender-Body Theory and Exact Solutions for Potential Flow Over an Ellipsoid," *Journal of Aircraft,* Vol. 27, No. 6, 1990, pp. 569–570.

[18]Wagner, H., "Über die Entstehung des dynamischen Auftriebes von Tragflügeln," *Zeitschrift fur Angewandte Mathematik und Mechanik,* Vol. 5, No. 1, 1925, pp. 17–35.

[19]von Kármán, T., and Sears, W. R., "Airfoil Theory for Non-Uniform Motion," *Journal of the Aeronautical Sciences,* Vol. 5, No. 10, 1938, pp. 379–390.

[20]McCune, J. E., Lam, C.-M. G., and Scott, M. T., "Nonlinear Aerodynamics of Two-Dimensional Airfoils in Severe Maneuver," *AIAA Journal,* Vol. 28, No. 3, 1990, pp. 385–393.

[21]Tavares, T. S., "Aerodynamics of Maneuvering Slender Wings with Leading-Edge Separation," Ph.D. Thesis, Dept. of Aeronautics and Astronautics, Massachusetts Inst. of Technology, Cambridge, MA, Sept. 1990.

[22]McCune, J. E., "Interactive Aerodynamics of Wings in Severe Maneuver," *Workshop II on Unsteady Separated Flow,* Air Force Technical Report FJSRL-TR-88-0004, July 1988, pp. 163–183.

[23]McCune, J. E., and Tavares, T. S., "Unsteady 3D Aerodynamics of Slender Wings in Severe Maneuver," 1st National Fluid Dynamics Congress, AIAA Paper 88-3544, Cincinnati, OH, July 1988.

[24]Dore, B. D., "The Unsteady Forces on Finite Wings in Transient Motion," British Aeronautical Research Council, ARCR&M, No. 3456, London, Sept. 1964.

[25]Jones, R. T., "The Unsteady Lift of a Wing of Finite Aspect Ratio," NACA Rept. 681, June 1939.

[26]Lamb, H., *Hydrodynamics,* 6th Ed., Dover, New York, 1945.

[27]Sarpkaya, T., "Computational Methods With Vortices—The 1988 Freeman Scholar Lecture," *Journal of Fluids Engineering,* Vol. 111, March 1989, pp. 5–52.

[28]Hoeijmakers, H. W. M., "Computational Aerodynamics of Ordered Vortex Flows," National Aerospace Laboratory, NLR Rept. TR 88088 U, Amsterdam, The Netherlands, 1988.

[29]Fink, P. T., and Taylor, J., "Some Early Experiments on Vortex Separation," British Aeronautical Research Council, ARCR&M, No. 3489, London, Sept. 1966.

[30]Shanks, R. E., "Low-Subsonic Measurements of Static and Dynamic Stability Derivatives of Six Flat-Plate Wings Having Leading-Edge Sweep Angles of 70° to 84°," NASA TN D-1822, April 1963.

[31]Tosti, L. P., "Low-Speed Static Stability and Damping-in-Roll Characteristics of Some Swept and Unswept Low-Aspect-Ratio Wings," NACA TN 1468, July 1947.

[32]Levin, D., and Katz, J., "Dynamic Load Measurements with Delta Wings Undergoing Self-Induced Roll Oscillations," *Journal of Aircraft,* Vol. 21, No. 1, 1984, pp. 30–36.

[33]Harvey, J. K., "A Study of the Flow Field Associated with a Steadily-Rolling Slender Delta Wing," *Journal of the Royal Aeronautical Society,* Vol. 68, No. 638, Feb. 1964, pp. 106–110.

[34]Lambourne, N. C., Bryer, D. W., and Maybrey, J. F. M., "The Behavior of the Leading-Edge Vortices Over a Delta Wing Following a Sudden Change of Incidence," British Aeronautical Research Council, ARCR&M No. 3645, London, March 1969.